

# Chiral spin-wave velocities induced by all-garnet interfacial Dzyaloshinskii-Moriya interaction in ultrathin yttrium iron garnet films

Hanchen Wang,<sup>1,\*</sup> Jilei Chen,<sup>1,2,\*</sup> Tao Liu,<sup>3,\*</sup> Jianyu Zhang,<sup>1</sup> Korbinian Baumgärtl,<sup>2</sup> Chenyang Guo,<sup>4</sup> Yuehui Li,<sup>5,6</sup> Chuanpu Liu,<sup>1,3</sup> Ping Che,<sup>2</sup> Sa Tu,<sup>1</sup> Song Liu,<sup>7</sup> Peng Gao,<sup>5,6,8</sup> Xiufeng Han,<sup>4</sup> Dapeng Yu,<sup>7,5</sup> Mingzhong Wu,<sup>3</sup> Dirk Grundler,<sup>2,9</sup> and Haiming Yu<sup>1,†</sup>

<sup>1</sup>*Fert Beijing Institute, BDBC, School of Microelectronics, Beihang University, Beijing 100191, China*

<sup>2</sup>*Laboratory of Nanoscale Magnetic Materials and Magnonics, Institute of Materials (IMX), School of Engineering,*

*École Polytechnique Fédérale de Lausanne (EPFL), 1015 Lausanne, Switzerland*

<sup>3</sup>*Department of Physics, Colorado State University, Fort Collins, Colorado 80523, USA*

<sup>4</sup>*Beijing National Laboratory for Condensed Matter Physics, Institute of Physics, University of Chinese Academy of Sciences, Chinese Academy of Sciences, Beijing 100190, China*

<sup>5</sup>*Electron Microscopy Laboratory, School of Physics, Peking University, Beijing 100871, China*

<sup>6</sup>*International Center for Quantum Materials, School of Physics, Peking University, Beijing 100871, China*

<sup>7</sup>*Shenzhen Institute for Quantum Science and Engineering (SIQSE), and Department of Physics, Southern University of Science and Technology (SUSTech), Shenzhen 518055, China*

<sup>8</sup>*Collaborative Innovation Center of Quantum Matter, Beijing 100871, China*

<sup>9</sup>*Institute of Microengineering (IMT), School of Engineering, École Polytechnique Fédérale de Lausanne (EPFL), 1015 Lausanne, Switzerland*  
(Dated: November 20, 2021)

Spin waves can probe the Dzyaloshinskii-Moriya interaction (DMI) which gives rise to topological spin textures, such as skyrmions. However, the DMI has not yet been reported in yttrium iron garnet (YIG) with arguably the lowest damping for spin waves. In this work, we experimentally evidence the interfacial DMI in a 7 nm-thick YIG film by measuring the nonreciprocal spin wave propagation in terms of frequency, amplitude and most importantly group velocities using all electrical spin-wave spectroscopy. The velocities of propagating spin waves show chirality among three vectors, i.e. the film normal direction, applied field and spin-wave wavevector. By measuring the asymmetric group velocities, we extract a DMI constant of  $16 \mu\text{J}/\text{m}^2$  which we independently confirm by Brillouin light scattering. Thickness-dependent measurements reveal that the DMI originates from the oxide interface between the YIG and garnet substrate. The interfacial DMI discovered in the ultrathin YIG films is of key importance for functional chiral magnonics as ultra-low spin-wave damping can be achieved.

Spin waves (or magnons) [1–3] are collective magnetic excitations that can propagate in metals [4] and also in insulators [5]. Intensive research efforts have been made to investigate spin waves in yttrium iron garnet  $\text{Y}_3\text{Fe}_5\text{O}_{12}$  (YIG) [6, 7] which exhibits the lowest damping that is promising for low-power consumption magnonic devices [8–10]. Most previous works were conducted on bulk or thick YIG films where the Damon-Eshbach (DE) spin-wave chirality [11–13] is well known for magnetostatic surface spin waves as illustrated in Fig. 1(a). However, the DE spin-wave chirality was negligible [14] in the thin YIG films which were recently achieved with high quality for on-chip magnonic devices [15, 16]. We report a different type of spin-wave chirality scaled up in ultrathin YIG films, which we attribute to the interfacial Dzyaloshinskii-Moriya interaction (DMI) [17, 18]. Very recently, domain wall motion in  $\text{Tm}_3\text{Fe}_5\text{O}_{12}$  (TmIG) on gadolinium gallium garnet  $\text{Gd}_3\text{Ga}_5\text{O}_{12}$  (GGG) suggested interfacial DMI consistent with the Rashba effect at oxide-oxide interfaces [19, 20]. However independent evidence for the DMI was not provided. Spin waves provide a prevailing method-

ology [21–27] for probing the DMI in metallic multilayers. DMI is the fundamental mechanism to form chiral spin textures, such as skyrmions [28–30]. Most previous studies on the interfacial DMI [23] focus on measuring frequency shifts  $\delta f$  between counter-propagating spin waves (with wavevectors  $+k$  and  $-k$ ) using Brillouin light scattering (BLS) [24, 26] or all-electrical spin-wave spectroscopy (AESWS) [25, 27]. Moon et al. [23] theoretically predicted the interfacial DMI to generate not only a frequency shift, but also asymmetric spin-wave group velocities. So far, there has been no experimental observation of nonreciprocal spin-wave characteristics and group velocities induced by interfacial DMI in bare ultrathin YIG films on GGG.

In this letter, we report chiral propagation of spin waves in a 7 nm-thick YIG film on a (111) GGG substrate [31]. The spin waves propagating in the chirally-favored direction are found to be substantially faster than in its counter direction as illustrated in Fig. 1(b). The asymmetry in group velocities  $\delta v_g$  is characterized by AESWS [4, 16, 25, 32] to be approximately 80 m/s. The chiral spin-wave velocities in YIG films can be accounted

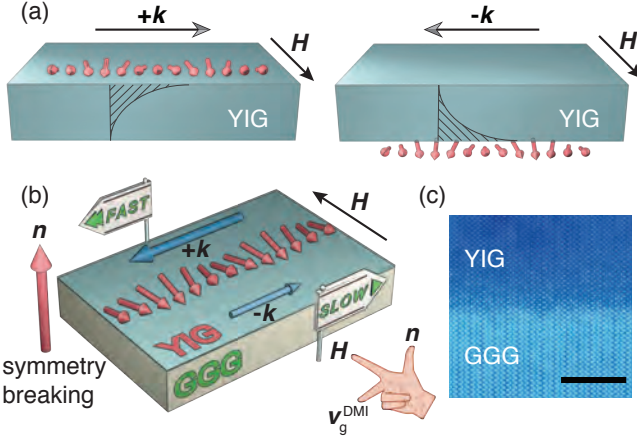


FIG. 1. (a) Damon-Eshbach spin-wave chirality in thick YIG films. (b) An illustrative diagram of the chiral propagation of spin waves in an ultrathin YIG film. The group velocities of spin waves propagating in  $+k$  and  $-k$  directions are different. The inset shows a right-handed chirality among three vectors, i.e. the film normal direction  $n$ , applied field  $H$  and DMI-induced drift group velocity  $v_g^{\text{DMI}}$ . (c) A high-angle annular dark-field image is taken at the YIG/GGG interface of the 7 nm-thick YIG sample. The scale bar is 5 nm.

for by an interfacial DMI [23] and a DMI constant of  $16 \mu\text{J}/\text{m}^2$  estimated from the experiments. By integrating different antennas, we vary the spin-wave wavevectors and obtain an asymmetric spin-wave dispersion that can be fitted well using the DMI constant extracted from the chiral spin-wave velocities. Five thin-film YIG samples with thicknesses of 7 nm, 10 nm, 20 nm, 40 nm and 80 nm are investigated. The DMI-induced  $\delta f$  [22, 23] and  $\delta v_g$  increase when the film thickness decreases, which demonstrates that the DMI in YIG is of interfacial type. We evidence the DMI in the ultrathin YIG films independently by BLS revealing nonreciprocal spin-wave dispersion relations. The DMI constants extracted from the BLS and the AESWS measurements performed on the 10 nm-thick YIG sample agree well. Our discovery makes chiral magnonics [33–35] a realistic vision as bare YIG offers ultra-low spin-wave damping and thereby enables the plethora of suggested devices that functionalize for instance unidirectional power flow, magnon Hall effect and nontrivial refraction of spin waves.

The YIG films were grown on GGG substrates by magnetron sputtering [31, 36]. The ferromagnetic resonance of the 7 nm-thick YIG film exhibits a narrow linewidth of 1 mT at 13 GHz and thereby the damping parameter is estimated to be 0.001 [36]. The DE spin-wave chirality [11–13] [Fig. 1(a)] is negligible when the thickness is 7 nm [14]. However, a new type of spin-wave chirality might arise in the presence of DMI where spin waves propagating in opposite directions not only show amplitude nonreciprocity and frequency shifts, but also chiral spin-wave velocities. They are attributed to

a DMI-induced drift group velocity whose direction follows a right-handed rule [inset of Fig. 1(b)] [35]. Figure 1(c) shows a high-angle annular dark-field image near the YIG/GGG interface. To measure the spin wave group velocities, two nano-striplines (NSLs) are integrated on the 7 nm-thick YIG film to excite and detect spin waves [36, 37]. The spin-wave propagation distance  $s = 2 \mu\text{m}$ . The spin-wave transmission spectra  $S_{12}$  ( $S_{21}$ ) suggest that spin waves are excited by NSL2 (NSL1) and detected by NSL1 (NSL2), which is defined as  $-k$  ( $+k$ ) spin-wave propagating directions [36]. The measured spectra with an external field swept from -50 mT to 50 mT are shown in Supplementary Material Fig. S3 [36]. Chiral propagation of spin waves is clearly observed with respect to the wavevector  $k$  and applied field  $H$ . This chirality is manifested in the angle-dependent measurement shown in Fig. 2. Figure 2(a) shows angle-dependent spectra for  $S_{12}$  ( $+k$ ), where a clear asymmetry is observed, i.e. the transmission spectrum for  $+90^\circ$  is substantially stronger than that of  $-90^\circ$ . The transmission spectra show contrast oscillations that indicate the phase variation of propagating spin waves [4, 16, 32]. In Fig. 2(b) we show a single spectrum at  $90^\circ$ , where a peak-to-peak frequency span  $\Delta f_+$  is marked indicating a phase change of  $2\pi$ . According to

$$v_g^{+(-)} = \frac{d\omega}{dk} = \frac{2\pi\Delta f_{+(-)}}{2\pi/s} = \Delta f_{+(-)} s, \quad (1)$$

the group velocity  $v_g^+$  for  $+k$  spin waves is estimated as  $v_g^+ \approx 312 \text{ m/s}$ , and the group velocity  $v_g^-$  for  $-k$  spin waves is estimated as  $v_g^- \approx 236 \text{ m/s}$ . Interestingly, for  $-90^\circ$ , i.e. a reversed applied field  $H$ , the situation is nearly mirrored (Fig. 2). This demonstrates that spin waves propagating in two counter directions ( $+k$  and  $-k$ ) exhibit different group velocities which can be reversed by changing the sign of the applied field and thereby chiral spin-wave velocities are observed.

Figure 3 shows  $\delta v_g = v_g^+ - v_g^-$  extracted from the field-dependent measurements [36] based on Eq. 1 as a function of the field applied in  $90^\circ$ . Near zero field, the group velocities reach about 560 m/s and are reciprocal. However, when the field increases, the group velocities for spin waves propagating in  $+k$  and  $-k$  directions become different. At positive fields,  $S_{12}$  is faster than  $S_{21}$  and at negative fields,  $S_{21}$  is faster than  $S_{12}$ , i.e. chiral spin-wave velocities are observed (Supplementary Material Fig. S4 [36]). The  $\delta v_g$  shows a distinctive step-like field dependence. Theoretical studies [23, 35] have predicted that interfacial DMI can introduce a drift group velocity  $v_g^{\text{DMI}}$ . We indeed observe  $v_g^{\text{DMI}}$  experimentally. We can extract  $v_g^{\text{DMI}} = 40.8 \text{ m/s}$  by fitting the experimental results in Fig. 3 with an empirical equation

$$\delta v_g = 2v_g^{\text{DMI}} \tanh\left(\frac{H}{H_0}\right), \quad (2)$$

where  $H_0$  is a fitting field value above which the velocity

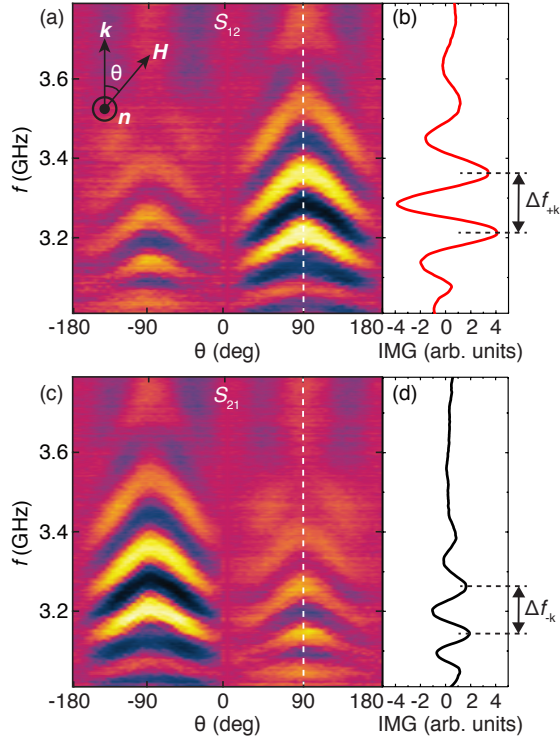


FIG. 2. Spin-wave transmission spectra  $S_{12}$  (a) and  $S_{21}$  (c) measured as a function of the field angle  $\theta$ . The field is fixed at 44 mT.  $\theta$  is defined as the angle between  $H$  and the  $k$ . Single spectra at  $90^\circ$  (dashed lines in (a) and (c)) are shown for  $S_{12}$  (b) and  $S_{21}$  (d). The peak-to-peak frequencies  $\Delta f_+ \approx 0.15$  GHz and  $\Delta f_- \approx 0.11$  GHz are extracted for the estimation of spin-wave group velocities  $v_g^+$  and  $v_g^-$ . The 260 nm-wide striplines are used in the experiments [36].

difference saturates. The sign of  $v_g^{\text{DMI}}$  is determined by a chiral relation among three unit vectors, i.e. the film normal vector  $\hat{\mathbf{n}}$ , applied field  $\hat{\mathbf{H}}$ , and spin-wave wavevector  $\hat{\mathbf{k}}$  [inset of Fig. 1(b)]. According to previous theoretical studies [23, 35], one can write

$$v_g^{\text{DMI}} = \left[ (\hat{\mathbf{n}} \times \hat{\mathbf{H}}) \cdot \hat{\mathbf{k}} \right] \frac{2\gamma}{M_S} D, \quad (3)$$

where  $D$  the DMI constant,  $M_S$  saturation magnetization. At a positive field, for example, the drift group velocity is towards the  $+k$  direction and therefore the spin-

wave group velocity in the  $+k$  direction is faster than in the  $-k$  direction. Consequently,  $\delta v_g$  shows a positive sign and is twice the  $v_g^{\text{DMI}}$ . Based on Eq. 3 and considering an  $M_S = 141$  kA/m [31], we can deduce a DMI constant  $D = 16 \mu\text{J}/\text{m}^2$ . The origin of a finite  $H_0$  is however unclear. It is higher than the coercive field characterized by the vibrating sample magnetometer [36]. In addition, the results of micromagnetic simulations [38] (green dashed line in Fig. 3) shows a step-like field dependence [36]. We speculate that  $H_0$  is related to a DMI-induced effective field that the external field needs to overcome before saturation is established.

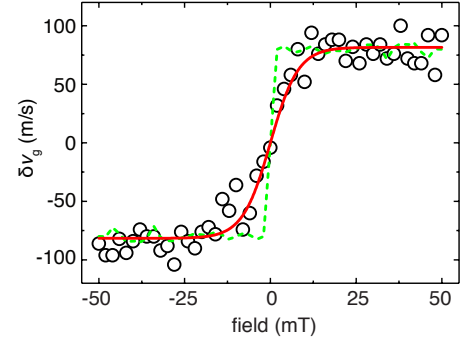


FIG. 3. The asymmetric group velocity  $\delta v_g = v_g^+ - v_g^-$  as a function of the applied field. The field is swept from -50 mT to 50 mT. Black circles are data points calculated using the values of  $v_g^+$  and  $v_g^-$  extracted from experiments [36]. The red line is a fit using Eq. 2. The green dashed line is the micromagnetic simulation results [36].

To study the  $k$  dependence, we integrated coplanar waveguides (CPWs) on the 7 nm-thick YIG film [36]. In spin-wave transmission spectra [36], two distinct modes are observed that are attributed to the CPW excited  $k_1 = 3.1$  rad/ $\mu\text{m}$  and  $k_2 = 9.1$  rad/ $\mu\text{m}$  modes, identified by the CPW Fourier transformation [4, 16, 25, 32, 36]. We can read out the  $k_1$  and  $k_2$  mode frequencies for both  $S_{12} (+k)$  and  $S_{21} (-k)$  from experimental data [36]. We summarize data points from NSL and CPW samples in Fig. 4(a) and observe clearly asymmetric characteristics. The spin-wave dispersion relation  $f(k)$  [Fig. 4(a)] can be calculated based on

$$f = \frac{\gamma\mu_0}{2\pi} \left[ \left( H + \frac{2A}{\mu_0 M_S} k^2 \right) \left( H + M_S + \frac{2A}{\mu_0 M_S} k^2 \right) + \frac{M_S^2}{4} (1 - e^{-2kt}) \right]^{\frac{1}{2}} + \left[ (\hat{\mathbf{n}} \times \hat{\mathbf{H}}) \cdot \hat{\mathbf{k}} \right] \frac{\gamma D}{\pi M_S} k, \quad (4)$$

where  $\gamma$  the gyromagnetic ratio,  $A = 0.37 \times 10^{-11}$  J/m the exchange stiffness constant [40],  $t = 7$  nm the film thickness. The first term is the non-chiral contribution

from the dipole-exchange spin waves [39] in a DE configuration [11, 40]. The second term originates from the interfacial DMI [23]. The chirality is determined

by the vector relation  $(\hat{\mathbf{n}} \times \hat{\mathbf{H}}) \cdot \hat{\mathbf{k}}$  and its amplitude is decided by the DMI strength  $D$ . By taking the DMI constant  $D = 16 \mu\text{J}/\text{m}^2$  extracted from  $\delta v_g$ , the calculated dispersion relations agree reasonably well with the experimental data points [Fig. 4(a)]. We rotate  $H$  in the film plane with respect to  $k$  and measure  $\delta v_g$  as a function of  $\theta$  [Fig. 4(b)]. The sinusoidal angular dependence is observed consistent with the vector relation  $(\hat{\mathbf{n}} \times \hat{\mathbf{H}}) \cdot \hat{\mathbf{k}}$  in the chiral term of the dispersion (second term of Eq. 4).  $\delta v_g$  becomes zero at  $0^\circ$  indicating a backward volume (BV) configuration [36]. In addition to the 7 nm-thick YIG film, we also measured spin-wave propagation in YIG films with other thicknesses [36]. The thickness dependence of  $\delta v_g$  is shown in Fig. 4(c), where the asymmetry in group velocities enlarges with decreasing thickness. This observation indicates that the observed DMI is an interfacial effect. The DMI constant  $D$  can then be expressed as  $D = \frac{\lambda D_i}{t}$  [25], where  $D_i$  the interfacial DMI parameter and  $\lambda$  the characteristic length of the interface, which depends on the details of the interface, such as roughness. With a rough estimation of  $\lambda$  being the lattice constant of YIG  $a = 12.4 \text{ \AA}$  [41] and a linear fitting of Fig. 4(c), we derive an interfacial DMI parameter  $D_i = 90 \mu\text{J}/\text{m}^2$ . The DMI-induced frequency shifts  $\delta f$  [22–26] are also observed [36].

The transmission spectra shown in Fig. 2 exhibit a clear amplitude nonreciprocity. The nonreciprocity parameter  $\beta = \frac{S_{12} - S_{21}}{S_{12} + S_{21}}$  is defined for quantitative analysis. Figure 4(d) shows the angle dependence of  $\beta$  on the 10 nm-thick YIG sample. At  $\theta = 0$ , the spin-wave propagation is nearly reciprocal because the BV mode is investigated [12]. At  $\theta = 90^\circ$ , the nonreciprocity increases when films go thicker [36] due to the DE nonreciprocity [14]. Interestingly, an unexpected increase of nonreciprocity occurs around  $30^\circ$  [Fig. 4(d)] [36], which may result from the interfacial DMI. The spin-wave dispersions for DE mode ( $90^\circ$ ), BV mode ( $0^\circ$ ) and an intermediate mode ( $30^\circ$ ) are calculated [36, 39]. In the low  $k$  limit, the group velocity evolves from positive to negative values when the field is rotated from the DE to BV configurations. At  $30^\circ$ , the dispersion becomes rather flat and therefore only a small group velocity  $v_g^0$  remains. If the DMI-induced drift group velocity  $v_g^{\text{DMI}} \approx v_g^0$ , the group velocity  $v_g^- = v_g^{\text{DMI}} - v_g^0$  becomes zero, but  $v_g^+ = v_g^{\text{DMI}} + v_g^0$  is non-zero. As a result, the nonreciprocity is enhanced due to the interfacial DMI [35, 36, 42].

We confirmed the interfacial DMI in ultrathin YIG films independently by BLS. The BLS spectra measured on the 10-nm thick YIG showed clear frequency shifts  $\delta f$  between the Stokes and Anti-Stokes peaks [36], indicating an asymmetric dispersion  $f(k)$  induced by the DMI. We extract  $\delta f$  from the BLS data and plot them as a function of the spin-wave wavevector  $k$

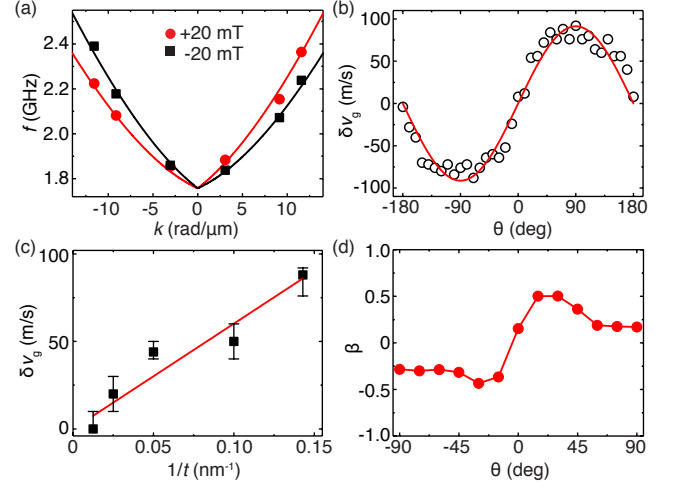


FIG. 4. (a) The asymmetric spin-wave dispersion in the presence of an interfacial DMI. The red dots (black squares) are experimental data extracted with an applied field of +20 mT (-20 mT). The red line (black line) is the calculated dispersion using a DMI constant of  $16 \mu\text{J}/\text{m}^2$  for +20 mT (-20 mT). (b) Angle-dependent asymmetric group velocities  $\delta v_g$ .  $\theta$  is defined in Fig. 2(a), where  $90^\circ$  ( $0^\circ$ ) indicates a DE (BV) configuration. The field is set at 44 mT. Black open circles are data points extracted from the experiments and the red line is a sinusoidal fitting. (c)  $\delta v_g$  for samples with different thicknesses of 7 nm, 10 nm, 20 nm, 40 nm and 80 nm with an applied field of 20 mT. The red line is a linear fit to the experimental data. (d) Spin-wave amplitude nonreciprocity  $\beta$  measured as a function of  $\theta$  on the 10 nm-thick sample. The field is fixed at 10 mT. The 730 nm-wide striplines are used in the experiments [36].

in Fig. 5, where  $\delta f$  increases with an increasing  $k$ . This is consistent with the linear relationship given by  $\delta f = \frac{2\gamma}{\pi M_S} D k$  [22–26]. Fitting the  $k$  dependent frequency shifts we extract a DMI constant of  $10.3 \pm 0.8 \mu\text{J}/\text{m}^2$  for the 10 nm-thick sample. This value is in good agreement with  $9.9 \pm 1.9 \mu\text{J}/\text{m}^2$  extracted from the chiral spin-wave velocities measured by the AESWS [Fig. 4(c)].

We now discuss the origin of the interfacial DMI in ultrathin YIG films. In general, the interfacial DMI stems from the inversion symmetry breaking in the film normal direction  $\hat{\mathbf{n}}$  and the spin-orbit coupling. In these samples, the upper surface is either exposed to air or covered by antennas, which are integrated on YIG films by evaporating 100 nm of Au starting with a thin Cr adhesion layer. One may suspect whether the Cr/YIG interface plays a role in generating the DMI. As a control measurement, we replace Cr by Ti and find that the chiral propagation of spin waves is similar [36]. This indicates that the DMI does not originate from the top but from the bottom surface of YIG consistent with TmIG/GGG samples reported recently [19, 20]. The DMI may be enhanced by adding a heavy metal layer [43, 44] on YIG, but consequently the damping will



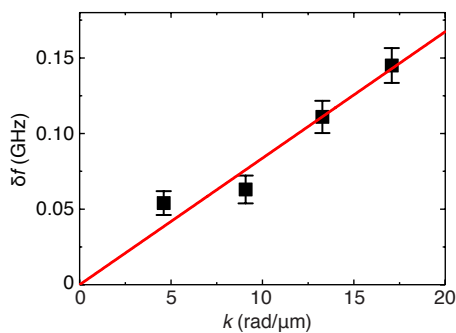


FIG. 5. Frequency shift  $\delta f$  (black squares) measured on the 10 nm-thick YIG sample in an applied field of 80 mT with BLS in reflection geometry at four different incident angles probing spin waves with wave vectors  $k = 4.6$  rad/ $\mu$ m, 9.1 rad/ $\mu$ m, 13.3 rad/ $\mu$ m and 17.1 rad/ $\mu$ m [36]. The red line is a linear fit to the experimental data.

be severely affected [45]. It has been found that ultrathin YIG grown on GGG by pulsed laser deposition may form a thin intermediate gadolinium iron garnet layer [46]. The energy dispersive X-ray spectroscopy and geometric phase analysis [36] are conducted and no significant Gd diffusion is found in the 7 nm-thick YIG film grown by sputtering. Therefore, Gd diffusion may not play the key role for generating the DMI. To fully understand the origin of the interfacial DMI at the YIG/GGG interface, more studies such as first-principles calculations [47, 48] and X-ray magnetic dichroism [49, 50] are required, which are beyond the scope of this work.

To summarize, we have observed chiral spin-wave velocities in ultrathin YIG films induced by DMI attributed to the YIG/GGG interface. The drift group velocity is about 40 m/s yielding a DMI constant of 16  $\mu$ J/m<sup>2</sup>. The chirality is ruled by the vector relation  $(\hat{n} \times \hat{H}) \cdot \hat{k}$ , verified by angle-dependent measurements. The DMI-induced chiral propagation of spin waves in the magnetic insulator YIG offers great prospects for chiral and spin-texture based magnonics [51–53].

The authors thank R. Duine, M. Kuepferling and A. Slavin for their helpful discussions and H.-Z. Wang for her help on the illustration. Financial support by NSF China under Grant Nos. 11674020 and U1801661, 111 talent program B16001, the National Key Research and Development Program of China No. 2016YFA0300802 and 2017YFA0206200, ANR-12-ASTR-0023 Trinidad and by SNF via project 163016 and sinergia grant 171003 Nanoskymionics is gratefully acknowledged. T.L. and M.W. were supported by the U.S. National Science Foundation (EFMA-1641989) and the U.S. Department of Energy, Office of Science, Basic Energy Sciences (DE-SC0018994). Y.L. and P.G. were supported by National Natural Science Foundation of China (51672007, 11974023), and The Key R&D Program of Guangdong

Province (2018B030327001, 2018B010109009).

\* These authors contributed equally to this work.

† haiming.yu@buaa.edu.cn

- [1] V.V. Kruglyak, S.O. Demokritov, and D. Grundler, Magnonics. *J. Phys. D: Appl. Phys.* **43**, 264001 (2010).
- [2] A.V. Chumak, V.I. Vasyuchka, A.A. Serga, and B. Hillebrands, Magnon spintronics. *Nat. Phys.* **11**, 453-461 (2015).
- [3] V.E. Demidov, S. Urazhdin, G. de Loubens, O. Klein, V. Cros, A. Anane, and S. O. Demokritov, Magnetization oscillations and waves driven by pure spin currents. *Phys. Rep.* **673**, 1-23 (2017).
- [4] V. Vlamincik, and M. Bailleul, Current-induced spin-wave Doppler shift. *Science* **322**, 410 (2008).
- [5] Y. Kajiwara, K. Hari, S. Takahashi, J. Ohe, K. Uchida, M. Mizuguchi, H. Umezawa, H. Kawai, K. Ando, K. Takanashi, S. Maekawa, and E. Saitoh, Transmission of electrical signals by spin-wave interconversion in a magnetic insulator. *J. Phys. D: Appl. Phys.* **464**, 262-266 (2010).
- [6] A.A. Serga, A.V. Chumak, and B. Hillebrands, YIG magnonics. *J. Phys. D: Appl. Phys.* **43**, 264002 (2010).
- [7] L. J. Cornelissen, J. Liu, R.A. Duine, J.B. Youssef, and B.J. van Wees, Long-distance transport of magnon spin information in a magnetic insulator at room temperature. *Nat. Phys.* **11**, 1022-1026 (2015).
- [8] A. Khitun, M. Bao, and K. L. Wang, Magnonic logic circuits. *J. Phys. D: Appl. Phys.* **43**, 264005 (2010).
- [9] T. Schneider, A. A. Serga, B. Leven, B. Hillebrands, R. L. Stamps, and M. P. Kostylev, Realization of spin-wave logic gates. *Appl. Phys. Lett.* **92**, 022505 (2008).
- [10] G. Csaba, A. Papp, and W. Porod, Perspectives of Using Spin Waves for Computing and Signal Processing. *Phys. Lett. A* **11**, 948-953 (2016).
- [11] R. W. Damon, and J. R. Eshbach, Magnetostatic modes of a ferromagnet slab. *J. Phys. Chem. Solids* **19**, 308 (1961).
- [12] V. E. Demidov, M.P. Kostylev, K. Rott, P. Krzytetzko, G. Reiss, and S.O. Demokritov, Excitation of microwaveguide modes by a stripe antenna. *Appl. Phys. Lett.* **95**, 112509 (2009).
- [13] K. Yamamoto, G.C. Thiang, P. Pirro, K.-W. Kim, K. Everschor-Sitte, and E. Saitoh, Topological characterization of classical waves: the topological origin of magnetostatic surface spin waves. *Phys. Rev. Lett.* **122**, 217201 (2019).
- [14] K.L. Wong, L. Bi, M. Bao, Q. Wen, J.P. Chatelon, Y.-T. Lin, C.A. Ross, H. Zhang, and K.L. Wang, Unidirectional propagation of magnetostatic surface spin waves at a magnetic film surface. *Appl. Phys. Lett.* **105**, 232403 (2014).
- [15] H. Chang, P. Li, W. Zhang, T. Liu, A. Hoffmann, L. Deng, and M. Wu, Nanometer-thick yttrium iron garnet films with extremely low damping. *IEEE Magn. Lett.* **5**, 6700 (2014).
- [16] H. Yu, O. Allivy Kelly, V. Cros, R. Bernard, P. Bortolotti, A. Anane, F. Brandl, R. Huber, I. Stasinopoulos, and D. Grundler, Magnetic thin-film insulator with ultra-low spin wave damping for coherent nanomagnonics. *Sci.*

- Rep. **4**, 6848 (2014).
- [17] I.A. Dzyaloshinsky, A thermodynamic theory of weak ferromagnetism of antiferromagnetics. *J. Phys. Chem. Solids* **4**, 241-255 (1958).
  - [18] T. Moriya, New mechanism of anisotropic superexchange interaction. *Phys. Rev. Lett.* **4**, 228-230 (1960).
  - [19] C.O. Avci, E. Rosenberg, L. Caretta, F. Büttner, M. Mann, C. Marcus, D. Bono, C.A. Ross, and G.S.D. Beach, Interface-driven chiral magnetism and current-driven domain walls in insulating magnetic garnets. *Nat. Nanotechnol.* **14**, 561-566 (2019).
  - [20] S. Ding, A. Ross, R. Lebrun, S. Becker, K. Lee, I. Bovenster, S. Das, Y. Kurokawa, S. Gupta, J. Yang, G. Jakob, and M. Kläui, Interfacial Dzyaloshinskii-Moriya interaction and chiral magnetic textures in a ferrimagnetic insulator. *Phys. Rev. B* **100**, 100406(R) (2019).
  - [21] Kh. Zakeri, Y. Zhang, J. Prokop, T.-H. Chuang, N. Sakr, W.X. Tang, and J. Kirschner, Asymmetric spin-wave dispersion on Fe(110): direct evidence of the Dzyaloshinskii-Moriya interaction. *Phys. Rev. Lett.* **104**, 137203 (2010).
  - [22] D. Cortés-Ortuño, and P. Landeros, Influence of the Dzyaloshinskii-Moriya interaction on the spin-wave spectra of thin films. *J. Phys.: Condens. Matter* **25**, 156001 (2013).
  - [23] J.-H. Moon, S.-M. Seo, K.-J. Lee, K.-W. Kim, J. Ryu, H.-W. Lee, R.D. McMichael, and M.D. Stiles, Spin-wave propagation in the presence of interfacial Dzyaloshinskii-Moriya interaction. *Phys. Rev. B* **88**, 184404 (2013).
  - [24] H.T. Nembach, J.M. Shaw, M. Weiler, E. Jué, and T.J. Silva, Linear relation between Heisenberg exchange and interfacial Dzyaloshinskii-Moriya interaction in metal films. *Nat. Phys.* **11**, 825-829 (2015).
  - [25] J.M. Lee, C. Jang, B.-C. Min, S.-W. Lee, K.-J. Lee, and J. Chang, All-electrical measurement of interfacial Dzyaloshinskii-Moriya interaction using collective spin-wave dynamics. *Nano Lett.* **16**, 62-67 (2016).
  - [26] X. Ma, G. Yu, S.A. Razavi, S.S. Sasaki, X. Li, K. Hao, S.H. Tolbert, K.L. Wang, and X. Li, Dzyaloshinskii-Moriya Interaction across an Antiferromagnet-Ferromagnet Interface. *Phys. Rev. Lett.* **119**, 027202 (2017).
  - [27] J. Lucassen, C.F. Schippers, M.A. Verheijen, P. Fritsch, E.J. Geluk, B. Barcones, R.A. Duine, S. Wurmehl, H.J.M. Swagten, B. Koopmans, and R. Lavrijsen, Extraction of Dzyaloshinskii-Moriya interaction from propagating spin waves validated. *arXiv:1909.02467*.
  - [28] S. Mühlbauer, B. Binz, F. Jonietz, C. Pfleiderer, A. Rosch, A. Neubauer, R. Georgii, and A.K. Schmid, Skyrmion lattice in a chiral magnet. *Science* **323**, 915 (2009).
  - [29] X.Z. Yu, Y. Onose, N. Kanazawa, J.H. Park, J.H. Han, Y. Matsui, N. Nagaosa, and Y. Tokura, Real-space observation of a two-dimensional skyrmion crystal. *Nature* **465**, 901 (2010).
  - [30] J. Sampaio, V. Cros, S. Rohart, A. Thiaville, and A. Fert, Nucleation, stability and current-induced motion of isolated magnetic skyrmions in nanostructures. *Nat. Nanotechnol.* **8**, 839 (2013).
  - [31] T. Liu, H. Chang, V. Vlaminc, Y. Sun, M. Kabatek, A. Hoffmann, L. Deng, and M. Wu, Ferromagnetic resonance of sputtered yttrium iron garnet nanometer films. *J. Appl. Phys.* **115**, 87-90 (2014).
  - [32] S. Neusser, G. Durr, H. G. Bauer, S. Tacchi, M. Madami, G. Woltersdorf, G. Gubbiotti, C. H. Back, and D. Grundler, Anisotropic propagation and damping of spin waves in a nanopatterned antidot lattice. *Phys. Rev. Lett.* **105**, 067208 (2010).
  - [33] A. Hrabec, M. Belmeguenai, A. Stashkevich, S.M. Chérif, S. Rohart, Y. Roussigné, and A. Thiaville, Making the Dzyaloshinskii-Moriya interaction visible. *Appl. Phys. Lett.* **110**, 242402 (2017).
  - [34] J. Mulkers, B. Van Waeyenberge, and M. V. Milošević, Tunable Snell's law for spin waves in heterochiral magnetic films. *Phys. Rev. B* **97**, 104422 (2018).
  - [35] J.-V. Kim, R.L. Stamps, and R.E. Camley, Spin wave power flow and caustics in ultrathin ferromagnets with the Dzyaloshinskii-Moriya interaction. *Phys. Rev. Lett.* **117**, 197204 (2016).
  - [36] See Supplemental Material for the FMR characterization of the 7 nm-thick YIG film, an SEM image on the sample with NSLs, the field-dependent spin wave measurement on the sample with NSLs, and on the sample with CPWs. Spin wave group velocities extracted from  $S_{12}$  and  $S_{21}$  as a function of the applied field. The magnetization characterization by the VSM. The results of the micromagnetic simulations. The spectra measured at the BV configuration. The field dependent spectra measured on samples with different thicknesses. The DMI-induced frequency shift measured as a function of the thickness. The spectra measured by 730 nm-wide NSLs. Angle-dependent nonreciprocity measured on samples with different thicknesses. Nonreciprocity shown in single spectra and the calculated dispersion at  $0^\circ$ ,  $30^\circ$  and  $90^\circ$ . The control measurement replacing Cr by Ti as the adhesion layer. EDX and GPA characterization at the YIG/GGG interface. The BLS spectra measured at different incident angles.
  - [37] F. Ciubotaru, T. Devolder, M. Manfrini, C. Adelman, and I.P. Radu, All electrical propagating spin wave spectroscopy with broadband wavevector capability. *Appl. Phys. Lett.* **109**, 012403 (2016).
  - [38] M. Donahue, and D. Porter, OOMMF Users Guide, Version 1.0, National Institute of Standards and Technology, Gaithersburg, MD, interagency report nistir 6376 Edition (Sept 1999). URL <http://math.nist.gov/oommf>.
  - [39] B.A. Kalinikos, and A.N. Slavin, Theory of dipole-exchange spin wave spectrum for ferromagnetic films with mixed exchange boundary conditions. *J. Phys. C: Solid State Phys.* **19**, 7013-7033 (1986).
  - [40] D.D. Stancil, and A. Prabhakar, *Spin Waves: Theory and Applications*. Appendix C, Springer (2009).
  - [41] M. Wu, A. Hoffmann, R.E. Camley, and R.L. Stamps, *Solid State Physics: Recent advances in magnetic insulators from spintronics to microwave applications*, 64 Academic Press (2013).
  - [42] T. Brächer, O. Boulle, G. Gaudin, and P. Pirro, Creation of unidirectional spin-wave emitters by utilizing interfacial Dzyaloshinskii-Moriya interaction. *Phys. Rev. B* **95**, 064429 (2017).
  - [43] X. Ma, G. Yu, C. Tang, X. Li, C. He, J. Shi, K.L. Wang, and X. Li, Interfacial Dzyaloshinskii-Moriya interaction: effect of 5d band filling and correlation with spin mixing conductance. *Phys. Rev. Lett.* **120**, 157204 (2018).
  - [44] Q. Shao, Y. Liu, G. Yu, S.K. Kim, X. Che, C. Tang, Q.L. He, Y. Tserkovnyak, J. Shi, and K.L. Wang, Topological Hall effect at above room temperature in heterostructures composed of a magnetic insulator and a heavy metal. *Nat. Electron.* **2**, 182-186 (2019).
  - [45] Y. Sun, H. Chang, M. Kabatek, Y.-Y. Song, Z. Wang, M.

- Jantz, W. Schneider, M. Wu, E. Montoya, B. Kardasz, B. Heinrich, S.G.E. teVelthuis, H. Schultheiss, and A. Hoffmann, Damping in yttrium iron garnet nanoscale films capped by platinum. *Phys. Rev. Lett.* **111**, 106601 (2013).
- [46] J.M. Gomez-Perez, S. Vélez, L. McKenzie-Sell, M. Amado, J. Herrero-Martín, J. López-López, S. Blanco-Canosa, L.E. Hueso, A. Chuvilin, J.W.A. Robinson, and F. Casanova, Synthetic antiferromagnetic coupling between ultrathin insulating garnets. *Phys. Rev. Applied* **10**, 044046 (2018).
- [47] I.V. Maznichenko, S. Ostanin, A. Ernst, and I. Mertig, Tunable 2D electron gas at the LaAlO<sub>3</sub>/SrTiO<sub>3</sub>(001) interface. *Phys. Rev. Mater.* **3**, 074006 (2019).
- [48] H. Yang, G. Chen, A.A.C. Cotta, A.T. N'Diaye, S.A. Nikolaev, E.A. Soares, W.A.A. Macedo, K. Liu, A.K. Schmid, A. Fert, and M. Chshiev, Significant Dzyaloshinskii-Moriya interaction at graphene/ferromagnet interfaces due to the Rashba effect. *Nat. Mater.* **17**, 605-609 (2018).
- [49] P. Yu, J.-S. Lee, S. Okamoto, M.D. Rossell, M. Huijben, C.-H. Yang, Q. He, J.X. Zhang, S.Y. Yang, M.J. Lee, Q.M. Ramasse, R. Erni, Y.-H. Chu, D.A. Arena, C.-C. Kao, L.W. Martin, and R. Ramesh, Interface ferromagnetism and orbital reconstruction in BiFeO<sub>3</sub>-La<sub>0.7</sub>Sr<sub>0.3</sub>MnO<sub>3</sub> heterostructures. *Phys. Rev. Lett.* **105**, 027201 (2010).
- [50] I. Hallsteinsen, A. Grutter, M. Moreau, S.D. Sløetjes, K. Kjærnes, E. Arenholz, and T. Tybell, Role of antiferromagnetic spin axis on magnetic reconstructions at the (111)-oriented La<sub>0.7</sub>Sr<sub>0.3</sub>MnO<sub>3</sub>/LaFeO<sub>3</sub> interface. *Phys. Rev. Mater.* **2**, 084403 (2018).
- [51] T. Schwarze, J. Waizner, M. Garst, A. Bauer, I. Stasinopoulos, H. Berger, C. Pfleiderer, and D. Grundler, Universal helimagnon and skyrmion excitations in metallic, semiconducting and insulating chiral magnets. *Nat. Mater.* **14**, 478-483 (2015).
- [52] K. Wagner, A. Kákay, K. Schultheiss, A. Henschke, T. Sebastian, and H. Schultheiss, Magnetic domain walls as reconfigurable spin-wave nanochannels. *Nat. Nanotechnol.* **11**, 432-436 (2016).
- [53] S. J. Hämäläinen, M. Madami, H. Qin, G. Gubbiotti, and S. van Dijken, Control of spin-wave transmission by a programmable domain wall. *Nat. Commun.* **9**, 4853 (2018).